Pseudo-Updated Constrained Solution Algorithm for Nonlinear Heat Conduction

Surapong Tovichakchaikul* and Joseph Padovan†
The University of Akron, Akron, Ohio

This paper develops efficiency and stability improvements in the incremental successive substitution (ISS) procedure commonly used to generate the solution to nonlinear heat conduction problems. This is achieved by employing the pseudo-update scheme of Broyden, Fletcher, Goldfarb and Shanno in conjunction with the constrained version of the ISS. The resulting algorithm retains the formulational simplicity associated with ISS schemes while incorporating the enhanced convergence properties of slope driven procedures as well as the stability of constrained approaches. To illustrate the enhanced operating characteristics of the new scheme, the results of several benchmark comparisons are presented.

Introduction

In recent years, with the advent of general-purpose finite difference (FD) and finite element (FE) codes,[1] the solution of large-scale heat conduction problems is certainly more commonplace. The use of such codes is not without pitfalls. For instance, in attempting to employ, say, the FE scheme, the user must select such items as[2] element type, mesh configuration, the number of quadrature points, and, for nonlinear problems, the thermal load step size. While linear simulations may be expensive for large-scale models, order of magnitude increases in cost are possible for nonlinear problems. This is a direct outgrowth of the iterative nature of the solution of such problems.

The most commonplace schemes employed to solve nonlinear steady state problems involve the use of either: 1) algebraic equation solvers such as the modified incremental successive substitution (MISS)/Newton Raphson (MINR) algorithms; or 2) direct numerical integration via, say, explicit/implicit schemes.

Generally speaking, many of the older finite difference type simulation codes such as CINDA [3] employ direct integration to yield steady-state solutions. In the more recent finite element type codes, such as NASTRAN (Cosmic[4]/MSC[5]) and ADINAT,[6] algebraic solvers are employed. This latter option has generally been employed by engineers in the solid mechanics community, since it is a natural outgrowth of numerical experiences associated with structural behavior. This is coupled with the fact that, as compared to direct integration, the algebraic equation solver approach usually requires many fewer trial-and-error user manipulations to obtain converged steady limiting solutions.

In this context, the current paper will be concerned with the stability and efficiency enhancement of algebraic equation solver schemes. Note that, due to the difficulty of calculating and handling the unsymmetric Jacobian matrix associated with the INR scheme,[8,9] the most widely used algorithm in general purpose (GP) codes such as NASTRAN[4,5] and ADINAT[6] is the MISS.[4-6] Recently, in an attempt to improve the stability and efficiency of the MISS, Padovan and Tovichakchaikul[7] have developed a so-called constrained version of this algorithm, namely the CMISS. The overall procedure employs an elliptic constraint curve to bound successive iterates, thereby enabling the use of large-scale load step sizes, and improving solution efficiency and stability. As has been shown in Ref. 7, the CMISS offers order-of-magnitude improvements over the straight version of the procedure.

In spite of such enhancements, if nonlinear analysis is to truly make an impact on engineering design calculations, significantly improved schemes will be required. In this context, this paper will introduce further improvements to the computational efficiency of the CMISS algorithm. This is achieved by employing the Broyden,[10,11] Fletcher,[12] Goldfarb,[13] and Shanno[14] (BFGS) pseudo-update[15-16] scheme to enhance the convergence characteristics of the procedure. The resulting BFGS updated CMISS algorithm retains the formulational simplicity associated with the MISS scheme while incorporating the enhanced convergence properties of slope-driven algorithms. Furthermore, since constraint conditions are still employed to bound the size of successive iterates, the overall scheme possesses improved convergence as well as stability characteristics.

To illustrate the overall numerical characteristics of the combined BFGS-CMISS scheme, the results of several benchmark problems will be presented. These will include comparisons of stability and efficiency with such schemes as the MISS and CMISS.

Governing Equations

Assuming the possibility of anisotropic conductivity properties, the governing heat equation takes the form

$$-b_{i,i}+Q=0 \tag{1}$$

where the heat flux vector b_i is defined by

$$b_i=-K_{ij}(T)\,T_{,j} \tag{2}$$

such that Q is the heat generation, T the temperature, and K_{ij} the conductivity tensor. The boundary conditions associated with Eqs. (1) and (2) are given by

$$\text{a) on } \partial R_T: \quad T=T \tag{3}$$

$$\text{b) on } \partial R_b: \quad b_i n_i=H_C(T-T_\infty)+H_R(T^4-T_\infty^4) \tag{4}$$

such that

$$\partial R=\partial R_T+\partial R_b \tag{5}$$

where ∂R denotes the boundary of R; H_C and H_R are, respectively, convective and radiative coefficients; and T_∞ is the appropriate ambient temperature.

Received Feb. 22, 1982; revision received Aug. 9, 1982.

*Research Associate, Department of Mechanical Engineering.
†Professor, Department of Mechanical Engineering.

To recast Eqs. (1-4) into the requisite FE formulation, T is written in shape function format, namely[2,7,8]

$$T=[N(x_1,x_2,x_3)]'T \tag{6}$$

where N is the shape function and T the nodal temperature. Employing either Galerkin's technique[8] or the appropriate variational principle, Eq. (6) can be used to establish the following assembled FE formulation:

$$[K(T)]T=Q \tag{7}$$

such that

$$[K(T)]=\int_R [B]'[K(T)][B]\,dv \tag{8}$$

$$Q=\int_R NQ\,dv \tag{9}$$

where

$$[K(T)]=\begin{vmatrix} K_{11} & K_{12} & K_{13} \\ K_{12} & K_{22} & K_{23} \\ K_{13} & K_{23} & K_{33} \end{vmatrix} \tag{10}$$

$$[B]=(N_{,1},N_{,2},N_{,3}) \tag{11}$$

Solution Algorithm

In terms of Eq. (7), the algorithm associated with the straight or modified successive substitution schemes (SS/MSS) takes the form

$$[K(T_j)]T_{i+1}=Q \tag{12}$$

or more simply

$$T_{i+1}=[K(T_j)]^{-1}Q \tag{13}$$

where for the SS, $j=i$ (continuous updating) and for the MSS, $j<i$ (intermediate updating).

Interpreted geometrically, successive iterations of Eq. (13) and its incremental versions trace out the procedural steps depicted by one-dimensional analogies given in Fig. 1. While the overall SS scheme is simple to implement, it has several shortcomings. Specifically, the procedure:

1) Does not provide an intrinsic means to bound successive iterates.

2) Cannot stably handle changes in curvature definiteness.

3) Does not provide a means to self-adaptively adjust load step size so as to improve the stability of the convergence process.

4) Generally requires extremely small load step sizes to accommodate zones of rapidly changing solution curvature.

To enhance the efficiency as well as stability of the ISS/MISS, Padovan and Tovichakchaikul[7] recently developed a constrained version, namely the CISS/CMISS. To introduce the concept of constraints, it is appropriate to reinterpret the ISS/MISS as a scheme that involves the intersection of an open constraint with an "extrapolation" of the solution curve. Note that much of the sensitivity associated with the ISS/MISS scheme can be directly attributed to the lack of a guarantee of such an intersection, as well as to the inability of controlling the growth of successive iterates. This is an outgrowth of the use of open constraints defined here by the prescribed external load given here by the hyperline $Q=Q_p$ illustrated in Fig. 1. Such a difficulty can be avoided by employing closed constraints. Specifically, the

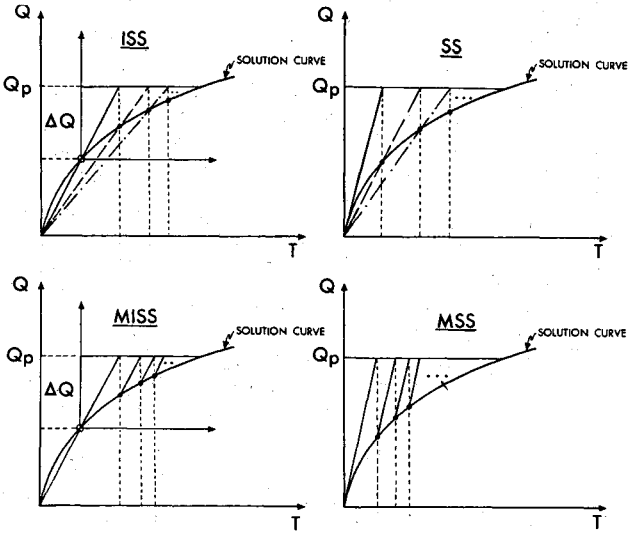

Fig. 1 One-dimensional analogies of SS, MSS, ISS, and MISS algorithms.

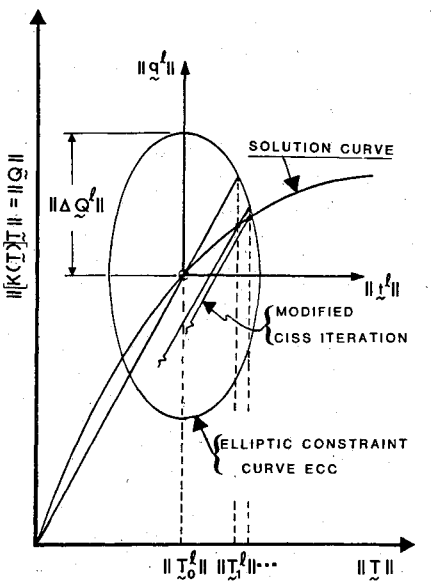

Fig. 2 Constrained modified incremental successive substitution scheme CMISS.

closeness property guarantees an intersection of the solution and bounding curve.

For the current purposes, following the approach of Ref. 7, an elliptic type constraint is employed. In terms of the geometry depicted in Fig. 2, the equation defining the constraint condition is given by the expression

$$\mu\|t_n^\ell\|^2+\|q_n^\ell\|^2=\|\Delta Q^\ell\|^2 \tag{14}$$

where

$$q_n^\ell=\lambda_n^\ell\Delta Q^\ell \tag{15}$$

$$t_n^\ell=T_n^\ell-T_0^\ell \tag{16}$$

$$\|(\ )\|=\sqrt{(\ )'(\ )} \tag{17}$$

such that the ℓ/n super/subscripts designate the load step and associated iteration count. Based on Eq. (14) and the standard MISS type iteration algorithm, it follows that

$$T_n^\ell=T_{n-1}^\ell-[K(T_0^\ell)]^{-1}\{\lambda_n^\ell\Delta Q^\ell+Q^\ell-[K(T_{n-1}^\ell)]T_{n-1}^\ell\} \tag{18}$$

where λ_n^ℓ defines a single parameter scaling of the incremental load vector $\Delta \boldsymbol{Q}^\ell$. It is determined from the elliptic constraint expression given by Eq. (14). The main function of λ_n^ℓ is to provide a bound on the admissible load excursion $\Delta \boldsymbol{Q}^\ell$ and thereby limit the size of successive iterations $\Delta \boldsymbol{T}_n^\ell$. It can be determined from the elliptic constraint expression given by Eq. (14). In this context, after several manipulations involving Eqs. (14) and (18), we have

$$\lambda_n^\ell = \frac{1}{2A_n^\ell} \{ -B_n^\ell \pm ((B_n^\ell)^2 - 4A_n^\ell C_n^\ell)^{1/2} \} \tag{19}$$

where

$$A_n^\ell = \mu \| [K(\boldsymbol{T}_0^\ell)]^{-1} \Delta \boldsymbol{Q}^\ell \|^2 + \| \Delta \boldsymbol{Q}^\ell \|^2 \tag{20}$$

$$B_n^\ell = 2\mu \langle [K(\boldsymbol{T}_0^\ell)]^{-1} \Delta \boldsymbol{Q}^\ell, [K(\boldsymbol{T}_0^\ell)]^{-1} \times (\boldsymbol{Q}^\ell - [K(\boldsymbol{T}_{n-1}^\ell)]\boldsymbol{T}_{n-1}^\ell) + \boldsymbol{T}_{n-1}^\ell - \boldsymbol{T}_0^\ell \rangle \tag{21}$$

$$C_n^\ell = \mu \| [K(\boldsymbol{T}_0^\ell)]^{-1} (\boldsymbol{Q}^\ell - [K(\boldsymbol{T}_{n-1}^\ell)]\boldsymbol{T}_{n-1}^\ell) + \boldsymbol{T}_{n-1}^\ell - \boldsymbol{T}_0^\ell \|^2 - \| \Delta \boldsymbol{Q}^\ell \|^2 \tag{22}$$

Since heat conduction problems typically preclude the existence of turning points, Eq. (19) is usually used in its "+" version, i.e., $\lambda_n^\ell = (\quad) + \sqrt{(\quad)}$.

Recently, Padovan and Arechaga[17,18] were able to prove formally that, for elliptically constrained INR and ISS algorithms for a purely real succession of λ_n^ℓ scaling factors, the overall iteration process is inherently convergent. This establishes the existence of a global safety zone defined by the discriminant of Eq. (19). Specifically, for real λ_n^ℓ it follows that

$$(B_n^\ell)^2 - 4A_n^\ell C_n^\ell \geq 0 \tag{23}$$

In terms of the form of Eqs. (20-23), we see that μ and $\Delta \boldsymbol{Q}^\ell$ can be self-adaptively updated to guarantee Eq. (23) and thus the convergence of the CMISS algorithm. For the present purposes this is achieved by letting the first iteration of a given load step size the abscissa dimension of the elliptic constraint. Specifically, the $\Delta \boldsymbol{T}_0^\ell$ excursion defines the abscissa and $\Delta \boldsymbol{Q}^\ell$ the ordinate. Thereafter, each CMISS iteration is checked against the safety zone condition defined by Eq. (23). If satisfied, the size/shape of the elliptic constraint remains fixed. If not, the ellipse is resized/shaped to ensure convergence. This is achieved by selecting a μ value which enforces the inequality defined in Eq. (23). For example, noting that $(B_n^\ell)^2$ and A_n^ℓ are positive definite, Eq. (23) is satisfied if $C_n^\ell < 0$; or, due to Eq. (22),

$$\mu < \frac{\| \Delta \boldsymbol{Q}^\ell \|^2}{\| [K(\boldsymbol{T}_0^\ell)]^{-1} (\boldsymbol{Q}^\ell - [K(\boldsymbol{T}_{n-1}^\ell)]\boldsymbol{T}_{n-1}^\ell) + \boldsymbol{T}_{n-1}^\ell - \boldsymbol{T}_0^\ell \|^2} \tag{24}$$

Equation (24) enables the resizing of the ellipse as the iteration process proceeds.

Beyond the self-adaptive attributes due to convergence characteristics, the CISS/CMISS schemes must always be applied in two main phases for problems involving specific applied thermal loads. The first involves the use of the CISS/CMISS algorithms, where the independent variables are applied in a manner typical of incrementation schemes. If no stability problems are encountered, then no adjustment occurs. Note that, due to the nature of the constraint, the intersection of the ellipse and the solution curve is not known a priori. Hence, incrementation of the first phase is continued until it follows that

$$\| [K(\boldsymbol{T}_0^\ell)]\boldsymbol{T}_0^\ell - \boldsymbol{Q}_p \| \leq \| \Delta \boldsymbol{Q} \| \tag{25}$$

where $\boldsymbol{Q}_p$ defines the prescribed thermal load. Once exceeded, it follows that the abscissa of the elliptic constraint curve ECC must be adjusted, hence initiating the second phase of the CISS/CMISS scheme. The adjusted load increment $\Delta \boldsymbol{Q}_a$ required by this phase is given by the expression

$$\Delta \boldsymbol{Q}_a = [K(\boldsymbol{T}_0^\ell)]\boldsymbol{T}_0^\ell - \boldsymbol{Q}_p \tag{26}$$

Figure 3 illustrates a one-dimensional analogy of the overall solution flow.

Due to its form, the CMISS has several very important advantages over the MISS, i.e.,[6]:

1) Successive iterates are automatically bound, thereby stabilizing the scheme.

2) Larger load steps can be employed, thereby enabling improved efficiency.

3) So-called safety zones exist wherein convergence is automatically guaranteed.[17,18]

4) Convergence can be guaranteed from a global basis since the safety zones can be self-adaptively expanded or contracted through the proper choice of μ and $\Delta \boldsymbol{Q}^\ell$.

To modify Eq. (18) to take advantage of the potentially faster convergence characteristics of slope-driven schemes such as the Newton-Raphson, the matrix $[K(\boldsymbol{T}_i^j)]$ is reinterpreted to be a pseudo-slope of the solution curve. Like the Newton-Raphson scheme, it can be updated during the course of iteration via the procedure derived by Broyden et al.[10-14] and recently termed the BFGS. Graphically, the overall flow of this procedure is depicted in Fig. 4.

As can be seen, the combined BFGS-CMISS scheme is applied in two main steps. The first involves the initial iteration CISS type estimate of the solution. Thereafter, the BFGS scheme is used to replace $[K(\boldsymbol{T}_i^j)]$ by a closer, continuously updated approximation of the solution curve's true slope and, therefore, more rapid convergence. This is clearly seen in the graphical juxtaposition of the CMISS and combined BFGS-CMISS scheme illustrated in Fig. 4.

In the context of the foregoing comments, Eq. (18) is recast in the form

$$\boldsymbol{T}_n^\ell = \boldsymbol{T}_{n-1}^\ell + [\Gamma_{n-1}^\ell] \{ \lambda_n^\ell \Delta \boldsymbol{Q}^\ell + \boldsymbol{Q}^\ell - [K(\boldsymbol{T}_{n-1}^\ell)]\boldsymbol{T}_{n-1}^\ell \} \tag{27}$$

where $[\Gamma_{n-1}^\ell]$ defines the pseudo-slope of the solution curve. At the start of the iteration process of a given load increment, $[\Gamma_{n-1}^\ell]$ takes the form

$$[\Gamma_0^\ell] = [K(\boldsymbol{T}_0^\ell)]^{-1} \tag{28}$$

Thereafter the BFGS scheme can be used to update $[\Gamma_{n-1}^\ell]$. Based on such a procedure, it follows that the $(n-1)$th BFGS update yields the expression[10-16]

$$[\Gamma_{n-1}^\ell] = [\phi_{n-1}^\ell]' [\Gamma_{n-2}^\ell] [\phi_{n-1}^\ell] \tag{29}$$

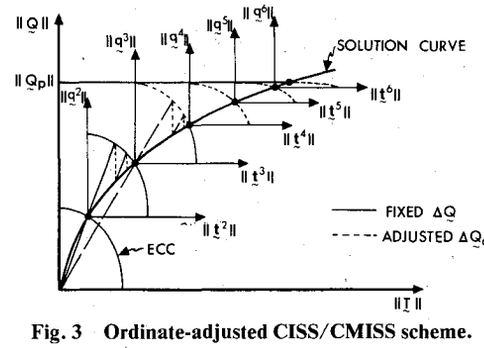

Fig. 3 Ordinate-adjusted CISS/CMISS scheme.

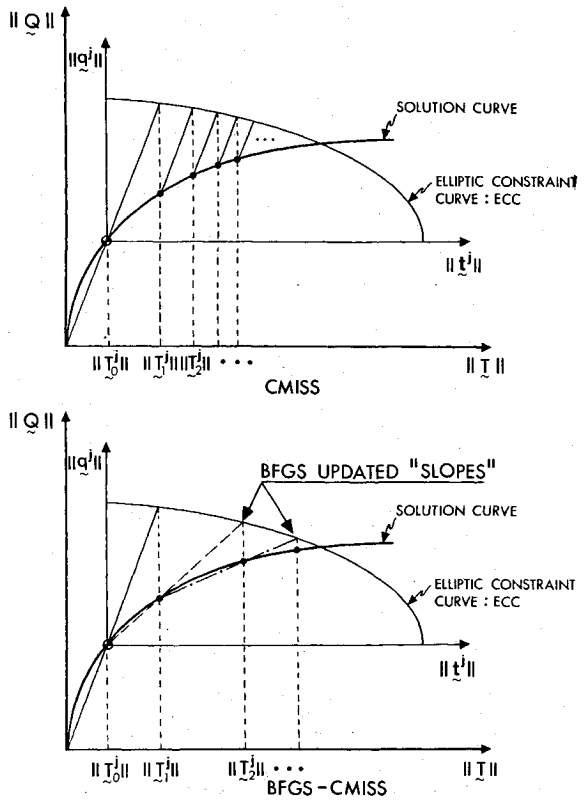

Fig. 4 Comparison of straight and BFGS updated CMISS.

where the pre- and post-multiplying matrix $[\phi_{n-1}]$ has the following structure

$$[\phi^{\ell}_{n-1}] = [I] + \boldsymbol{Z}^{\ell}_{n-1}(\boldsymbol{Y}^{\ell}_{n-1})' \tag{30}$$

such that the vectors $\boldsymbol{Z}^{\ell}_{n-1}$ and $\boldsymbol{Y}^{\ell}_{n-1}$ are defined by

$$\boldsymbol{Z}^{\ell}_{n-1} = -\left\{\frac{(\boldsymbol{U}^{\ell}_{n-1})'\boldsymbol{V}^{\ell}_{n-1}}{(\boldsymbol{U}^{\ell}_{n-1})'[\Gamma^{\ell}_{n-2}]\boldsymbol{U}^{\ell}_{n-1}}\right\}^{1/2}[\Gamma^{\ell}_{n-2}]\boldsymbol{U}^{\ell}_{n-1} - \boldsymbol{V}^{\ell}_{n-1} \tag{31}$$

$$\boldsymbol{Y}^{\ell}_{n-1} = \frac{\boldsymbol{U}^{\ell}_{n-1}}{(\boldsymbol{U}^{\ell}_{n-1})'\boldsymbol{V}^{\ell}_{n-1}} \tag{32}$$

with

$$\boldsymbol{U}^{\ell}_{n-1} = \boldsymbol{T}^{\ell}_{n-1} - \boldsymbol{T}^{\ell}_{n-2} \tag{33}$$

$$\boldsymbol{V}^{\ell}_{n-1} = [K(\boldsymbol{T}^{\ell}_{n-1})]\boldsymbol{T}^{\ell}_{n-1} - [K(\boldsymbol{T}^{\ell}_{n-2})]\boldsymbol{T}^{\ell}_{n-2} \tag{34}$$

Due to its structure, the $[\phi^{\ell}_{n-1}]$ appearing in Eq. (29) requires vector rather than full matrix multiplications. In this way, the updating of $[K(\boldsymbol{T}^{\ell}_{0})]$ is a very efficient calculation.

With regard to the foregoing BFGS updating, there are two basic ways to employ the overall BFGS-CMISS strategy. The first follows directly from the standard use of the MISS. Namely, the matrix $[K(\boldsymbol{T})]$ is updated at the beginning of each load step to yield $[K(\boldsymbol{T}^{\ell}_{0})]$. Thenceforth, BFGS type updating is employed to obtain $[\Gamma^{\ell}_{n-1}]$. Such a process yields the algorithms defined by Eqs. (27-34).

Alternatively, the matrix $[K(\boldsymbol{T})]$ is "updated" for the first load step and thereafter only on an intermittent basis. For all intervening load steps and associated iterations, the BFGS is used to continuously update $[\Gamma^{\ell}_{n-1}]$. For such an approach, Eq. (27) takes the form

$$\boldsymbol{T}^{\ell}_{n} = \boldsymbol{T}^{\ell}_{n-1} + [\Gamma^{\ell k}_{n-1}]\{\lambda^{\ell}_{n}\Delta\boldsymbol{Q}^{\ell} + \boldsymbol{Q}^{\ell} - [K(\boldsymbol{T}^{\ell}_{n-1})]\boldsymbol{T}^{\ell}_{n-1}\} \tag{35}$$

where

$$[\Gamma^{\ell k}_{n-1}] = ([\phi^{\ell}_{n-1}]\ldots[\phi^{\ell-1}_{m}]\ldots[\phi^{k}_{r}]\ldots)'[K(\boldsymbol{T}^{k}_{0})]^{-1} \times (\ldots[\phi^{k}_{r}]\ldots[\phi^{\ell-1}_{m}]\ldots[\phi^{\ell}_{n-1}]) \tag{36}$$

such that k defines the most recent update of the $[K(\boldsymbol{T})]$ matrix.

Note that, since Eq. (35) does not require the evaluation of the Jacobian matrix, it retains the simplicity of the original CMISS algorithm with only a slight increase in required computations caused by the use of the BFGS update. This will become clear in the series of benchmark problems discussed in the next section.

Benchmarking

In the preceding section, the CMISS algorithm was extended to include BFGS updating. This enabled the development of a combined algorithm which retains the formulational simplicity of the CMISS as well as the improved convergence associated with BFGS type updating. As noted during the development, two basic solution strategies were developed for the combined BFGS-CMISS scheme: 1) updating of $[K(\boldsymbol{T})]$ at the beginning of each load step and; 2) updating $[K(\boldsymbol{T})]$ for the first step and thereafter only on an intermittent basis to prevent potential drift.

Note either approach has the self-adaptive properties mentioned earlier. That is, based on the concept of safety zones,[17,18] the elliptic constraint curve can be resized during the course of calculation so as to guarantee convergence of the solution. Due to the inherent stability of the scheme, the thermal loading can be applied in a single step, which is thereafter self-adaptively adjusted during the iteration process.

To benchmark the inherent stability, efficiency, and accuracy of the combined BFGS-CMISS scheme, the results of a series of numerical experiments will now be presented. To extend the scope of testing, a variety of nonlinear conductivity types is considered. These include such "real-world" materials as epoxy,[19] copper germanium,[19] polyvinyl-chloride,[19] and zirconium-based ceramic coatings.[20] For evaluation purposes, the results of the combined BFGS-CMISS scheme will be compared to those generated by the straight CMISS and MISS procedures. This will be achieved by determining the number of load steps and associated iterations required to obtain a convergent solution. To extend the scope of testing, both one- and two-dimensional configurations will be considered.

In the context of the foregoing, Fig. 5 illustrates the configuration and associated boundary conditions used to perform the one-dimensional benchmarking. For the sake of consistency, the combined BFGS-CMISS, the straight CMISS, and the straight MISS were programmed into the ADINAT general-purpose finite element code. This enabled the use of identical equation solvers, element types, quadrature formulas, etc.

To start the comparison, Fig. 5 illustrates the conductivity properties of epoxy. Based on this material and the configuration defined in Fig. 5, Table 1 illustrates the effects of load step size on the number of iterations required to achieve converged solutions of the three aforementioned schemes. As can be seen, the combined BFGS-CMISS algorithm showed an order-of-magnitude improvement in solution efficiency for the same accuracy tolerance. Table 2 illustrates the required number of load steps and iterations for a given thermal load. Note that only one load step was required for the combined BFGS-CMISS algorithm to yield the solution. This compares with a minimum of 8 load steps for the CMISS and 15 for the MISS. As can be seen from Table 2, the associated numbers of iteration are 21 for the combined BFGS-CMISS, 91 for CMISS, and 261 for the MISS. The reason for the failure of the CMISS and MISS for load steps less than 8 and 15,

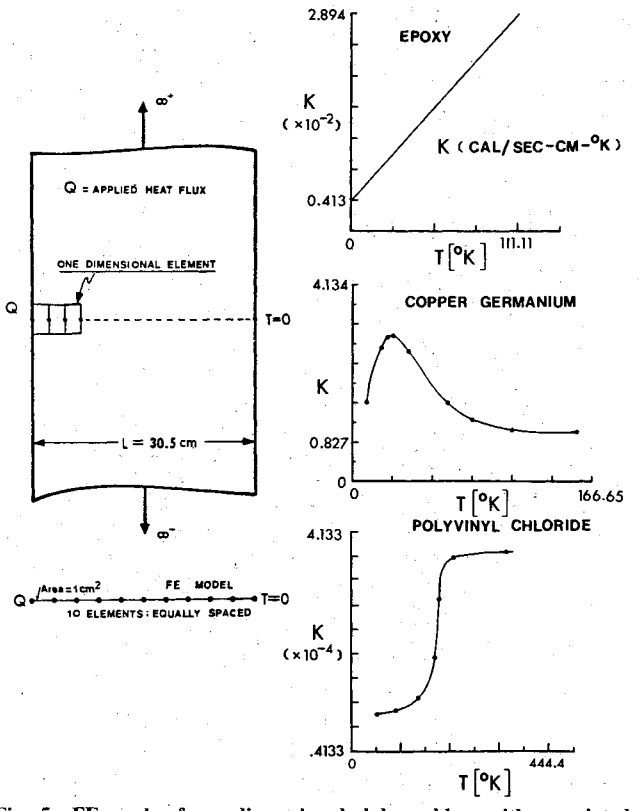

Fig. 5 FE mesh of one-dimensional slab problem with associated material properties.

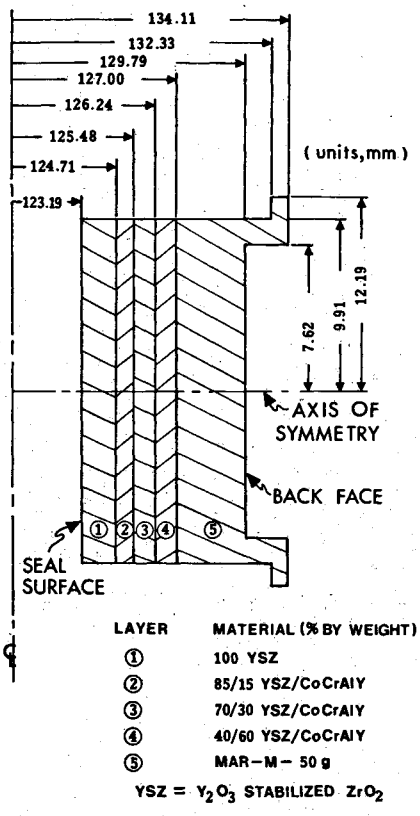

Fig. 6 Geometry of multilayered gas turbine seal (Ref. 20).

Table 1 Effects of load step size (ΔQ) on the number of required iterations: epoxy; tolerance = 10^{-4}

ΔQ W/cm^2	MISS	CMISS	BFGS/ CMISS
0.00847	18	12	6
0.00989	23	16	6
0.01224	43	27	7
0.01411	96	53	7
0.01537	—[a]	119	7
0.01695	—[a]	—[a]	8

[a] Failed by exceeding limit stop of 200 iterations.

Table 2 Comparison of number of iterations required for convergence: epoxy; total $Q = 0.218$ W/cm^2; tolerance = 10^{-4}

Number of load steps				
MISS		CMISS		BFGS/ CMISS
1-14	15	1-6	8	1
—[a]	261	—[a]	91	21

[a] Failed by exceeding limit stop of 200 iterations per given load step.

Table 3 Comparison of number of iterations required for convergence: copper germanium; total $Q = 25.02$ W/cm^2; tolerance = 10^{-4}

Load step	Number of iterations MISS 1	5	10	15	BFGS/CMISS 1
1	—[a]	—[a]	11	8	11
2			8	7	
3			7	6	
4			6	6	
5			5	6	
6			6	5	
7			7	5	
8			7	5	
9			7	5	
10			7	5	
11				5	
12				6	
13				6	
14				6	
15				6	
Total	—[a]	—[a]	71	87	11

[a] Failed by exceeding limit stop of 30 iterations.

respectively, follows from the fact that excessive increment size leads to drift. In this case, the solutions were stopped since, for a given load step, an iteration count of more than 200 was exceeded. Such sensitivity obviously leads to significant time-consuming user intervention to choose the proper load step size. This is in contrast to the combined BFGS-CMISS scheme, which required only one load step and significantly fewer iterations to converge.

Figure 5 illustrates the conductivity properties of copper germanium. Based on this material and the one-dimensional configuration, Table 3 illustrates the number of load steps and associated iterations required to yield converged solutions. As can be seen, the combined BFGS-CMISS yielded an order-of-magnitude improvement, i.e., 7 to 1. Finally, Fig. 5 also illustrates the conductivity properties of polyvinylchloride. In the context of the previous numerical experiments, Table 4 illustrates the comparison of efficiencies. As can be seen, the combined BFGS-CMISS required only one load step to yield the solution, while the CMISS and MISS required, respectively, 10 and 34 increments. The associated number of iterations are 21 for the combined BFGS-CMISS, 141 for the CMISS, and 551 for the MISS. This represents a 7 to 1 improvement over the CMISS and 26 to 1 over the MISS.

As a final example of the numerical characteristics of the BFGS-CMISS, we shall now consider the comprehensive two-dimensional problem depicted in Fig. 6. The configuration represents a cross-sectional view of a turbine seal whose thermal-mechanical behavior was recently considered by Ref.

20. As can be seen, the seal consists of several layers of zirconium-based ceramic bonded to a metallic substrate. One notes from Table 5 that the thermal properties of the various layers are highly temperature dependent.

Figure 7 illustrates the two-dimensional FE model of the seal. It involves 159 four-node two-dimensional elements and 1 five-node element. The boundary conditions associated with the seal are as follows:

1) Seal surface, convectively heated via hot combustion gases wherein $h = 5700$ W/m^2 K and $T_{gas} = 1644$ K.

2) Back face surface, convectively cooled via bypass air wherein $h = 1140$ W/m^2 K and $T_{gas} = 900$ K.

3) Other surfaces are insulated.

Based on the foregoing seal model, Table 6 illustrates comparisons between the MISS and BFGS-CMISS schemes. As noted earlier, these were programmed into ADINAT to keep all numerical and modeling procedures completely consistent. Noting the results depicted, it follows that, as with the previous one-dimensional examples, the BFGS-CMISS is inherently stable. In addition to requiring significantly fewer iterations to converge (1 to 4), only one load step was needed. This represents a significant improvement for the user since little judgment is necessary to guarantee convergence. The accuracy of the results obtained can be seen from the comparison given in Fig. 8 with the work of Ref. 20.

Discussion and Conclusion

In the context of the foregoing, it follows that the combined BFGS-CMISS scheme yields significantly improved operating characteristics over either the straight CMISS or especially the MISS. Specifically, as can be seen from the benchmark experiments, the scheme appears to possess significant advantages: 1) it is inherently stable, 2) computationally very efficient, 3) highly self adaptive and, 4) can be used in conjunction with very large load increments. Items 1, 3, and 4 are a direct outgrowth of the use of the elliptic solution constraint defined by Eq. (14). For example, the self adaptiveness of the combined BFGS-CMISS algorithm follows from the fact that the constraint surface used to bound successive iterations can be warped to guarantee convergence. As noted earlier, this is possible by monitoring whether the conditions of the safety zone are satisfied. Item 2, the computational efficiency, is a combination of both the use of the BFGS update and the stabilizing characteristics of the solution constraint associated with the CMISS.

Table 4 Comparison of number of iterations required for convergence: polyvinylchloride; total $Q = 0.0095$ W/cm^2; tolerance $= 10^{-4}$

	Number of iterations				
Load	MISS		CMISS		BFGS/CMISS
step	1-33	34	1-9	10	1
1	—[a]	5	—[a]	4	21
2		4		4	
3		4		7	
4		5		43	
5		6		24	
6		11		19	
7		13		16	
8		12		9	
9		14		6	
10		11		9	
⋮		⋮			
33		193			
34		44			
Total	—[a]	551	—[a]	141	21

[a] Failed by exceeding limit stop of 200 iterations.

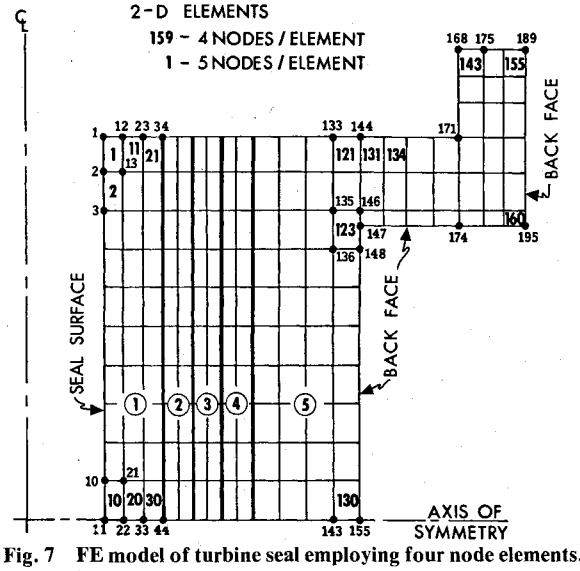

Fig. 7 FE model of turbine seal employing four node elements.

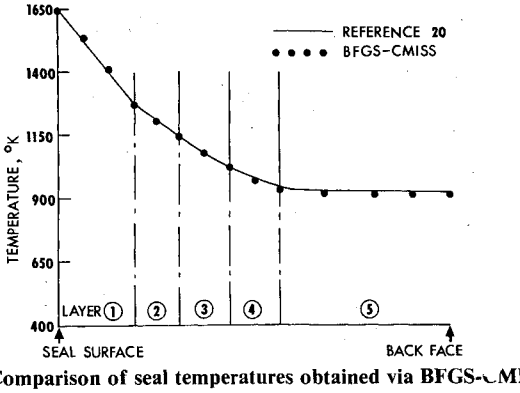

Fig. 8 Comparison of seal temperatures obtained via BFGS-CMISS scheme and Ref. 20.

Table 5 Thermal properties of various layers associated with turbine seal illustrated in Fig. 6

	Layer 1		Layer 2		Layer 3		Layer 4		Layer 5	
Property	Temp., K	Property	Temp., K	Property	Temp., K	Property	Temp., K	Property	Temp., K	Property
Density, kg/m^3	All	4290	All	4982	All	5674	All	7031	All	8858
Specific heat,	476	550	476	534	476	516	476	483	476	445
J/kg K	1366	646	1366	643	1366	638	1366	625	1366	609
Thermal	366	0.51	366	0.51	366	0.51	366	0.51	—	—
conductivity,	533	0.51	533	0.58	533	0.62	533	0.67	—	—
W/m K	811	0.54	811	0.78	811	0.93	811	1.04	—	—
	1089	0.59	1089	1.06	1089	1.32	1089	1.52	—	—
	1366	0.71	1366	1.45	1366	1.85	1366	2.20	—	—
	1644	1.01	1644	2.03	1644	2.61	1644	3.18	1644	52.7

Table 6 Comparison of required number of load steps and associated iterations for MISS and BFGS-CMISS algorithms

No. of load step	No. of iterations MISS	BFGS-CMISS
1	—[a]	12
2	—[a]	
3	—[a]	
4	—[a]	
5	—[a]	
6	—[a]	
7	—[a]	

[a] No convergence.

In closing, it should be noted that the combined BFGS-CMISS algorithm retains the formulational simplicity of the straight MISS. In this context it can easily be programmed into most general-purpose codes without the need of any significant rearchitecturing.

Acknowledgments

This work has been supported by NASA Lewis, under Grants NAG3-54 and NAG3-265. The second author is grateful to C. C. Chamis of NASA Lewis for the stimulating discussions and encouragement during the analytical phases of this work. Acknowledgment is also given to R. Hendriks of NASA Lewis for his enthusiastic stimulation of the authors in the area of high-temperature seals.

References

[1] Noor, A., "Survey of Computer Programs for Solutions of Nonlinear Structural and Solid Mechanics Problems," *Computers and Structures,* Vol. 13, 1981, p. 425.

[2] Zienkiewicz, O. C., *The Finite Element Method,* McGraw-Hill, New York, 1977.

[3] Gaski, J. D. and Lewis, D. R., "Chrysler Improved Numerical Differencing Analyzer: CINDA 3G," Chrysler Corp., Space Div., Rept. TN-AP-67-287, Oct. 1967.

[4] *The Nastran User Manual (level 17.6=COSMIC VERSION),* NASA SP-22(03), 1978.

[5] Schaeffer, H. G., *MSC/NASTRAN PRIMER Static and Normal Modes Analysis,* Schaeffer Analysis Inc., Mount Vernon, N.H., 1979.

[6] Bathe, K. C., "ADINAT: A Finite Element Program for Automatic Dynamic Incremental Nonlinear Analysis of Temperatures," MIT, Cambridge, Mass., Rept. 82448-5, 1978.

[7] Padovan, J. and Tovichakchaikul, S., "Self Adaptive Closed Constrained Solution Algorithms for Nonlinear Conduction," *Numerical Heat Transfer,* Vol. 5, 1982, pp. 253-274.

[8] Padovan, J., "Steady Heat Conduction in Linear and Nonlinear Fully Anisotropic Media by Finite Elements," *Journal of Heat Transfer, Transactions of ASME,* Vol. 90, 1974, pp. 313-318.

[9] Padovan, J., "Finite Element Analysis of Nonlinear Conduction Problems Subject to Moving Fields," *Numerical Heat Transfer,* Vol. 3, 1980, pp. 259-279.

[10] Broyden, C. G., "The Convergence of a Class of Double-Rank Minimization Algorithms, 1: General Considerations," *Journal of Institute of Mathematical Applications,* Vol. 6, 1970, pp. 76-90.

[11] Broyden, C. G., "The Convergence of a Class of Double Rank Minimization Algorithms, 2: The New Algorithm," *Journal of Institute of Mathematical Applications,* Vol. 6, 1970, pp. 222-231.

[12] Fletcher, B., "A New Approach to Variable Metric Algorithms," *Computer Journal,* Vol. 13, 1970, pp. 317-322.

[13] Goldfarb, D., "A Family of Variable-Metric Methods Derived by Variational Means," *Mathematical Computation,* Vol. 24, 1970, pp. 23-26.

[14] Shanno, D. F., "Conditioning of Quasi Newton-Methods for Function Minimization," *Mathematical Computation,* Vol. 24, 1970, pp. 647-656.

[15] Matthies, H. and Strang, G., "The Solution of Nonlinear Finite Element Equations," *International Journal of Numerical Methods in Engineering,* Vol. 14, 1979, p. 1612.

[16] Hughes, T. J. R., "Implicit-Explicit Finite Element Techniques for Symmetric and Nonsymmetric Systems," Presented at the International Conference on Numerical Methods for Nonlinear Problems, Swansea, 1980.

[17] Padovan, J. and Arechaga, T., "Formal Convergence Characteristics of Elliptically Constrained Incremental Newton Raphson Algorithms," *International Journal of Engineering Science,* Vol. 20, 1982, pp. 1077-1097.

[18] Padovan, J. and Arechaga, T., "Formal Numerical Characteristics of Closed Constrained Incremental Successive Substitution Algorithms," *Journal of the Franklin Institute,* Vol. 314, 1982, pp. 143-168.

[19] Goldsmith, A., Waterman, T. E., and Hirschorn, H. J., *Handbook of Thermophysical Properties of Solid Materials,* The MacMillan Co., New York, 1961.

[20] Taylor, C. M. and Bill, R. C., "Thermal Stresses in a Plasma-Sprayed Ceramic Gas Path Seal," *Journal of Aircraft,* Vol. 16, 1978, pp. 239-246.